Pressure-induced B1–B2 structural phase transition and elastic properties of $U_xLa_{1-x}S$ solid solution

2007 J. Phys.: Condens. Matter 19 346212

(http://iopscience.iop.org/0953-8984/19/34/346212)

IOP PUBLISHING JOURNAL OF PHYSICS: CONDENSED MATTER

J. Phys.: Condens. Matter **19** (2007) 346212 (19pp) doi:10.1088/0953-8984/19/34/346212

Pressure-induced B1–B2 structural phase transition and elastic properties of $U_xLa_{1-x}S$ solid solution

Dinesh Varshney[1,4], N Kaurav[2], R Kinge[1] and R K Singh[3]

[1] School of Physics, Vigyan Bhawan, Devi Ahilya University, Khandwa Road Campus, Indore 452001, India
[2] Department of Physics, Institute of Science and Laboratory Education, IPSA, Rajendra Nagar, Indore 452012, India
[3] Institute of Professional, Scientific Studies and Research, Choudhary Devi Lal University, Sirsa 125055, India

E-mail: vdinesh33@rediffmail.com

Received 3 May 2007, in final form 8 June 2007
Published 24 July 2007
Online at stacks.iop.org/JPhysCM/19/346212

Abstract

A comprehensive phenomenological calculation is reported for the pressure-dependent structural phase transition, equation of state and elastic properties of $U_xLa_{1-x}S$ solid solution. We develop an effective interionic interaction potential incorporating the long-range Coulomb and the Hafemeister and Flygare form of short-range overlap repulsion extended up to the second-neighbour ions and van der Waals (vdW) multipole interactions. The overlapping of the f orbitals with the p orbitals of the nearest neighbour in $U_xLa_{1-x}S$ that influences the effective Coulomb interactions is noticed to be a potential parameter in revealing the structural phase transition (from NaCl type (B1) to CsCl type (B2)) as well the equations of state of $U_xLa_{1-x}S$ ($x = 0, 0.08, 0.40, 0.50, 0.60, 0.80$ and 1.0) rare-earth compounds. The calculated results have revealed reasonably good agreement with the available data on the phase transition pressures (P_t = 25.5 (LaS), 30 ($U_{0.08}La_{0.92}S$), 34 ($U_{0.40}La_{0.60}S$), 35 ($U_{0.50}La_{0.50}S$), 47 ($U_{0.60}La_{0.40}S$), 59 ($U_{0.80}La_{0.20}S$) and 81 (US) GPa). The equation of state curves (plotted between $V(P)/V(0)$ and pressure) for both the NaCl-type (B1) and CsCl-type (B2) structures obtained by us are in fairly good agreement with the experimental results. Deduced values of the volume collapses [$\Delta V(P)/V(0)$] are also closer to their observed data. Further, the variations of the second- and third-order elastic constants with pressure have followed a systematic trend, that is almost identical to those exhibited by the measured and observed data in other compounds of NaCl-type structure family.

[4] Author to whom any correspondence should be addressed.

1. Introduction

Rare-earth compounds, especially uranium monochalcogenides ($5f^3$), attract considerable attention due to the intricate electronic properties relating to the highly correlated f electrons [1]. At ambient conditions the rare-earth monochalcogenides are characterized by a fixed f^n configuration of atomic-like f electrons. The application of pressure eventually decreases the lattice spacing, leading to the destabilization of the f shell. The rare-earth compounds such as $U_xLa_{1-x}S$ exhibit the simple rock salt structure; one can vary the uranium–uranium spacing to investigate the change in structural, electronic and magnetic behaviour as the degree of electron localization changes from localized to itinerant behaviour [2, 3], as a consequence of changes in the chemical environment.

Pressure is one of the external parameters by which the interplay of the f electrons with the normal conduction electrons may be varied. As the nature of the f-electron states depends on the f-orbital overlaps, these can be tuned in a controlled manner by changing the interatomic distance by applying external pressure [4]. Thus, the physical properties of the f-electron-based systems are substantially changed and studies on pressure effects in these systems appears to be quite exciting [5].

The rare-earth monopnictides and monochalcogenides are some of the structurally simplest materials, and numerous experimental works have studied the pressure behaviour of these compounds because high-quality single crystals have been prepared successfully. Muon spin relaxation measurements are powerful probes in determining the magnetic characteristics of materials with magnetic ions. Grosse *et al* have carried out muon spin rotation/relaxation (μ SR) measurements on single crystals of $U_xLa_{1-x}S$ in the temperature range between 0.1 and 300 K [6]. They argued that all compounds except the diamagnetic LaS exhibit a magnetic transition with the transition temperature decreasing linearly with diminishing uranium content. In addition, Schoenes *et al* have systematically studied the effect of diluting US with LaS, a pseudobinary compound, and found that the degree of localization varies non-monotonically and, in a certain range, contrary to the U–U separation [7]. Henceforth, hybridization and magnetic exchange play a dominant role in $U_xLa_{1-x}S$ rare-earth compounds.

The investigations of structural, mechanical and vibrational properties of semiconducting alloys under pressure are now routinely being performed by means of *ab initio* calculations. The accuracy of total energies obtained within the local density approximation is in many cases sufficient to predict which structure, at a given pressure, has the lowest free energy, although most calculations still refer to zero temperature. Furthermore, by comparing the free energies of various guessed crystal structures, *ab initio* molecular dynamics methods allow a better determination of the structures and understanding of transformation mechanisms, since they perform the structural optimizations. However, with the rapid advancement of computational techniques, the nature of interatomic forces is still not properly interpreted for these materials, and phenomenological lattice dynamical models, which take into account various interaction energies for the determination of stable structure, cover the chemical trends in the atomic characteristics.

For several years Cooper and his collaborators have performed *ab initio* calculations by assuming the existence of f–d hybridization in order to understand the magnetic properties of uranium compounds [8–11]. The first-principles calculations on hybridization effects [8] and a comparison of results for cerium and uranium show the difference between almost localized and almost itinerant magnetism for compounds of Ce and U, respectively. A newly proposed two-electron band theory approach could predict the Wilson ratio for heavy-fermion systems [9]. Moreover, the model of two kinds of uranium f electron, namely localized magnetic and itinerant nonmagnetic [11], explains quite well the drastic decay of the ordered moments by

alloying. As a proper reference material the effect of diluting US with LaS, the high-pressure structural properties of ULaS solid solutions have not been investigated in detail.

In any doped rare-earth compound, an understanding of its properties must be preceded by x-ray diffraction study of the doping impurities. Bihan *et al* performed x-ray diffraction measurements under pressure on seven different compositions in the $U_xLa_{1-x}S$ system ($x = 0, 0.08, 0.40, 0.50, 0.60, 0.80, 1.0$) with different pressure-transmitting media [12]. All the compounds have the NaCl-type (B1) structure at ambient pressure, but show different behaviour under pressure. Furthermore, for doping concentration $x \leqslant 0.60$ the compounds show a phase transformation from the ambient NaCl structure to the CsCl-type structure while, for $x \geqslant 0.60$, the high-pressure phase has yet to be determined. In addition, the structural and elastic studies on lanthanum mono-chalcogenides have further widened the scope of future theoretical and accurate experimental investigations of the crystallographic phase transition from B1 to B2 in rare-earth compounds [13, 14].

Among the lattice models which have been invoked so far to discuss the mechanical properties of several solids and alloys, the charge-transfer approach [15], following Hafemeister and Flygare type overlap repulsion has been extended up to second-neighbour ions besides short-range interactions [16]. We refer to the pioneering work of Fumi and Tosi, who properly incorporate van der Waals (vdW) interactions along with dipole–dipole (d–d) and dipole–quadrupole (d–q) interactions to reveal the cohesion in several ionic solids [17]. In trying to understand the structural aspects, we admit that the vdW attractions are the cornerstone of lattice phenomenological models that is ignored in the first-principles microscopic calculations.

Motivated from the earlier first-principles calculations [8, 11] and the phenomenological lattice models [15] for the successful description of the phase transition and high-pressure behaviour of several binary semiconductors, we thought it pertinent to employ the two-body interactions that include vdW attraction, which is not explicitly accounted for in the first-principles pseudopotential, for the estimation of structural and elastic properties in rare-earth monochalcogenides. We shall see that vdW interactions are effective in revealing the elastic and structural properties of these compounds. For this purpose we use an effective interionic potential model, proposed earlier, for the rare-earth compounds [13].

In trying to understand the structural and mechanical aspects of doped lanthanum monochalcogenides, we shall aim at assessing whether the developed effective interionic potential (EIoIP), which includes the effect of f-electron screening on the Coulomb interactions between the ions through a modified charge parameter, can explain the reported pressure-dependent behaviour in these compounds. We examine first the suitability of this potential to predict the NaCl to CsCl structure transformation in this group of rare-earth compounds. Later on we compute the phase transition pressures, relative volume changes and variations of second-order elastic constants with pressure with earlier developed potential.

The essentials of the lattice model and the method of computations are given in section 2. Theoretical results are compared and discussed with the existing first-principles, experimental, and predicted data, and are presented in section 3. A summary of results obtained in the previous section is presented in section 4.

2. Details of the model

The phenomenological lattice models for a solid-state structural transformation with hydrostatic pressures have been known in the thermodynamic limit. Usually, an increase in the static pressure on a crystal leads to a decrease in its volume. Thermodynamically, an isolated phase is stable only when its free energy is minimum for the specified conditions. As the temperature or pressure or any other variable acting on the systems is altered, the Gibbs

free energy changes smoothly and continuously. A phase transition is said to occur when the changes in structural details of the phase are caused by such variations of free energy.

The doped rare-earth monochalcogenides transform from their initial B1 (NaCl) to B2 (CsCl) structure under pressure. For this purpose, the Gibbs free energy is generically defined as follows:

$$G = U + PV - TS, \tag{1}$$

where U is the internal energy or lattice energy assumed to consist of the long-range Coulomb force which at 0 K corresponds to the cohesive energy, and S is the vibrational entropy at absolute temperature T, pressure P and volume V. Indeed, the static transition pressures have been obtained in the thermodynamic limit by solving for the pressure that makes the Gibbs free energies of both phases equal.

The structural phase stability of a particular structure is decided by the minima of the Gibbs free energy. Since these theoretical calculations are performed at $T = 0$ K, the Gibbs free energy became equal to the enthalpy, $H = U + PV$. For a given pressure, a stable structure is one for which thermodynamic potential (G or H) has its lowest value. We have estimated the Gibbs free energy for both the B1 and B2 phases. The Gibbs free energies of both phases are as follows:

$$G_{\mathrm{B1}}(r) = U_{\mathrm{B1}}(r) + PV_{\mathrm{B1}} \tag{2}$$

at $T = 0$ K for the rock salt (RS) B1 (real) phase and

$$G_{\mathrm{B2}}(r') = U_{\mathrm{B2}}(r') + PV_{\mathrm{B2}} \tag{3}$$

at $T = 0$ K for the CsCl (CC) B2 (hypothetical) phase. At the phase transition pressure P, the Gibbs free energy difference is $\Delta G[= G_{\mathrm{B2}}(r') - G_{\mathrm{B1}}(r)]$. Here, $V_{\mathrm{B1}} = 2r^3$ and $V_{\mathrm{B2}} = [8/3\sqrt{3}]r'^3$ as the unit cell volume for the B1 and B2 phase, respectively. The notations U_{B1} and U_{B2} denote cohesive energies of real B1 and hypothetical B2 phases, respectively, and are written as

$$U_{\mathrm{B1}}(r) = -\alpha\frac{\mathrm{e}^2 Z_{\mathrm{m}}^2}{r} + 6V_{ij}(r) + 6V_{ii}(r) + 6V_{jj}(r) \tag{4}$$

and

$$U_{\mathrm{B2}}(r') = -\alpha'\frac{\mathrm{e}^2 Z_{\mathrm{m}}^2}{r'} + 8V_{ij}(r') + 3V_{ii}(r') + 3V_{jj}(r'). \tag{5}$$

Here, $\alpha(=1.7475)$ and $\alpha'(=1.7627)$ are the Madelung constants for the NaCl and CsCl structure, respectively. The long-range Coulomb is represented by the first term; the second term corresponds to the Hafemeister and Flygare [16] form of short-range repulsive energies; and the van der Waals multipoles are represented by the third and fourth terms, respectively. The nearest-neighbour (nn) separation r (r') corresponds to the NaCl (CsCl) phase. As pointed out earlier, for the structural changes in uranium-doped rare-earth monochalcogenides, it is the pressure as an external parameter that influences the f-electron orbitals. It is then necessary to introduce some simplifying assumptions without loss of generality. We assume that Z_{m}^2 is the modified charge and parametrically includes the effect of Coulomb screening by the delocalized f electrons. The short-range repulsive potential (V_{ij}) (in equations (4) and (5)) for both the phases between the ions is as follows:

$$V_{ij} = b\beta_{ij}\exp\left(\frac{r_i + r_j - r_{ij}}{\rho}\right) + c_{ij}r_{ij}^{-6} + d_{ij}r_{ij}^{-8}; \qquad i, j = 1, 2, \tag{6}$$

b and ρ being the short-range parameters. The Pauling coefficients β_{ij} are defined as $\beta_{ij} = 1 + (Z_i/n_i) + (Z_j/n_j)$ with Z_i (Z_j) and n_i (n_j) as the valency and number of outermost

electrons, respectively [18]. We obtain $\beta_{ij} = 1.0$, $\beta_{ii} = 1.5$ and $\beta_{jj} = 0.5$, similar to values for most of the NaCl-type compounds. $r_i(r_j)$ are the cation (anion) radii. The symbols c_{ij} and d_{ij} are the van der Waals (vdW) coefficients. r_{ij} is the nearest-neighbour distance. The effective interionic potential can then have three free parameters: modified ionic charge (Z_m), range (b) and hardness (ρ), which can be determined from the known crystal properties. The last two terms in equation (6) are the van der Waals (vdW) energy due to dipole–dipole (d–d) and dipole–quadrupole (d–q) interactions.

The study of the second-order elastic constants (SOECs) (C_{11}, C_{12} and C_{44}) and their pressure derivatives at 0 K is quite important for understanding the nature of the interatomic forces in rare-earth chalcogenides as ULaS solid solutions. Since these elastic constants are functions of the first- and second-order derivatives of the short-range potentials, their calculations will provide a further check on the accuracy of short-range forces in these materials.

The effective interionic interaction potential (EIoIP) in equation (6) corresponds to a dynamical matrix in terms of force constants. The elements of the Coulomb, the repulsive interaction matrix are determined from the derivatives of EIoIP [19] and are then obtained for B1 by subjecting the dynamical matrix to the long-wavelength limit. The expressions for the SOECs for B1 phase are

$$C_{11} = \frac{e^2}{4r_0^4}\left[-5.112Z_m^2 + A_1 + \frac{(A_2 + B_2)}{2}\right], \tag{7}$$

$$C_{12} = \frac{e^2}{4r_0^4}\left[0.226Z_m^2 - B_1 + \frac{(A_2 - 5B_2)}{4}\right], \tag{8}$$

$$C_{44} = \frac{e^2}{4r_0^4}\left[2.556Z_m^2 + B_1 + \frac{(A_2 + 3B_2)}{4}\right], \tag{9}$$

where (A_1, B_1) and (A_2, B_2) are the short-range parameters for the nearest and the next-nearest neighbours, respectively, and are defined as

$$A_1 = \frac{4r_0^3}{e^2}\left[\frac{d^2}{dr^2}V_{ij}\right]_{r=r_0}, \tag{10}$$

$$A_2 = \frac{4(r_0\sqrt{2})^3}{e^2}\left[\frac{d^2}{dr^2}V_{ii} + \frac{d^2}{dr^2}V_{jj}\right]_{r=r_0\sqrt{2}}, \tag{11}$$

$$B_1 = \frac{4r_0^2}{e^2}\left[\frac{d}{dr}V_{ij}\right]_{r=r_0}, \tag{12}$$

$$B_2 = \frac{4(r_0\sqrt{2})^2}{e^2}\left[\frac{d}{dr}V_{ii} + \frac{d}{dr}V_{jj}\right]_{r=r_0\sqrt{2}}. \tag{13}$$

Here, V_{ij} and V_{ii} (V_{jj}) are the overlap potentials between the nearest and the next-nearest neighbours, respectively. $r_0\sqrt{2}$ denotes the next-nearest-neighbour distance in the B1 phase.

Given the effective interionic potential and its applications to various thermodynamic and elastic properties for the chosen material, we now began to estimate and compute numerically the high-pressure phase transition and elastic properties for the B1 phase.

3. Discussion and analysis of results

With application of pressure a new crystal phase appears in the materials and the relative stability of the two crystal structures naturally requires an extremely accurate prediction.

Table 1. The values of van der Waals coefficients c_{ij} $(i, j = 1, 2)$ (in units of 10^{-60} erg cm^6), d_{ij} $(i, j = 1, 2)$ (in units of 10^{-76} erg cm^8) and overall van der Waals coefficients (C, D) for $U_xLa_{1-x}S$ compounds.

Compound	c_{ii}	c_{ij}	c_{jj}	C	d_{ii}	d_{ij}	d_{jj}	D
LaS	35.2	98.6	305.1	957.7	20.4	86.8	332.9	674.7
$U_{0.08}La_{0.92}S$	29.8	90.7	305.1	900.8	17.3	79.8	332.9	630.8
$U_{0.40}La_{0.60}S$	12.6	59.2	305.1	677.2	7.3	52.1	332.9	456.1
$U_{0.50}La_{0.50}S$	8.8	49.3	305.1	608.7	5.1	43.4	332.9	401.9
$U_{0.60}La_{0.40}S$	5.6	39.4	305.1	540.8	3.2	34.7	332.9	347.8
$U_{0.80}La_{0.20}S$	1.4	19.7	305.1	406.9	0.82	17.3	332.9	240.2
US	7.8	45.5	395.0	663.9	3.02	50.5	570.9	540.0

Theoretical studies of cohesive, structural and vibrational properties of semiconductors under pressure are now accurately being performed by means of *ab initio* calculations. On the other hand, several empirical models suggest that the key for predicting relative structural energies is not absolute accuracy but to carefully incorporate the chemical trends in the atomic characteristics. It is widely believed that phenomenological models are interpretative rather than predictive of the stability of phases.

While discussing the stability of crystal structures and the pressure-induced phase transition theoretically it is essential to estimate the total free energy of crystals which consist of ions and valence electrons. The contributions from the system of electrons to the total energy of the crystal are intimately connected with the mechanism of cohesion and interatomic bonding in the crystals. We need to determine the most stable structure at finite pressure and temperature in terms of the thermodynamic potential as Gibbs free energy $G = U + PV - TS$. The structure with lowest free energy is the most stable. However, it is difficult to minimize the free energy from randomly generated structures even with highly sophisticated computational techniques. To further simplify our calculations, the temperature has been set to zero, i.e., the entropy of the crystal is therefore ignored. It may be mentioned here that the contribution of temperature to free energy is small for the experimental data considered.

The effective interionic potential (EIoIP) is constructed in a hierarchical and easily generalizable manner so that the structural and elastic properties are interpreted in an ordered way. For such purposes we have then three material-dependent parameters, namely the modified ionic charge, range and hardness (Z_m, ρ and b), which have been evaluated from the equilibrium condition [19]

$$\left|\frac{\mathrm{d}U(r)}{\mathrm{d}r}\right|_{r=r_0} = 0 \tag{14}$$

and the bulk modulus (B_T):

$$\left|\frac{\mathrm{d}^2U(r)}{\mathrm{d}r^2}\right|_{r=r_0} = (9kr_0)^{-1}B_T \tag{15}$$

using the experimental values of lattice constant and bulk modulus (B_T).

The values of the van der Waals (vdW) coefficients (c_{ij} and d_{ij}) and the overall vdW coefficients (C and D) have been evaluated from the well-known Slater–Kirkwood variational method [20] and are listed in table 1. It is worth pointing out that the values of the vdW coefficients depend on the polarization and ionic radii and hence there is a difference in the vdW coefficients of LaS and $U_xLa_{1-x}S$. We consider all the compounds to be partially ionic.

It is instructive to point out that the mixed crystals, according to the virtual crystal approximation [21], are regarded as an array of average ions whose masses, force constants

Table 2. Crystal data and model parameters for $U_xLa_{1-x}S$ compounds.

	Material parameters				Model parameters		
Compounds	r_i (Å)	r_j (Å)	a_0 (Å)	B_T (GPa)	Z_m^2	b (10^{-12} erg)	ρ (10^{-1} Å)
LaS	1.04[a]	1.24[a]	5.852[b]	89[c]	3.18	7.83	3.05
US	0.80[a]	1.24[a]	5.489[d]	90[e]	2.924	9.48	3.07
$U_{0.08}La_{0.92}S$					2.56	7.962	3.052
$U_{0.40}La_{0.60}S$					2.856	8.49	3.058
$U_{0.50}La_{0.50}S$					2.924	8.655	3.06
$U_{0.60}La_{0.40}S$					3.43	8.82	3.062
$U_{0.80}La_{0.20}S$					3.92	9.15	3.066

[a] Reference [23].
[b] Reference [24].
[c] Reference [12].
[d] Reference [1].
[e] Reference [25].

and effective charges are considered to scale linearly with concentration. These facts allow us to first estimate the material parameters for both binary compounds. We can now pay particular attention for the doping in lanthanum monochalcogenides. In what follows we assume that these parameters vary linearly with the doping concentration (x), and hence Vegard's law [22] is appropriate:

$$b(U_xLa_{1-x}S) = (1-x)b(LaS) + xb(US), \tag{16}$$

and

$$\rho(U_xLa_{1-x}S) = (1-x)\rho(LaS) + x\rho(US). \tag{17}$$

The input data for undoped and doped uranium chalcogenides with their relevant references and the deduced model parameters from the knowledge of ionic radii [23], equilibrium distance (r_0), the bulk modulus (B_T) and the Cauchy violation (C_{12}–C_{44}) are given in table 2. It is perhaps worth remarking that we have deuced the values of the material parameters modified ionic charge (Z_m^2), hardness (b) and range (ρ) from the knowledge of the equilibrium distance [1, 24] and the bulk modulus [12, 25] following the equilibrium conditions [19]. The input data along with their relevant references and the model parameters for $U_xLa_{1-x}S$ compounds are given in table 2. The consistency between model calculations and reported values of phase transition pressures is attributed to the facts that the ionic charge parameters vary non-monotonically with concentration in $U_xLa_{1-x}S$.

Figure 1 shows the variation of modified ionic Z_m^2 of $U_xLa_{1-x}S$ compounds as a function of concentration (x). It is inferred from the plot that the value of Z_m^2 is lower for lower doping concentration of U and increases with higher x. For $x \cong 0.0$, i.e. LaS, $x \cong 0.5$, i.e. $U_{0.5}La_{0.5}S$ and $x \cong 1.0$, i.e. US, the value of Z_m^2 is nearly the same. This can be readily understood by considering their electronic structure. In the domain ($0.0 < x < 0.5$), the number of f-electron sites is less as compared to higher x, while the reverse is true for the doping concentration range $0.5 < x < 1.0$. Hence, for low U concentration the system $U_xLa_{1-x}S$ shows a highly delocalized nature, while for higher U, the system shows more stable f^3 sites. It is worth commenting that the valence state of U ions changes around the critical concentration $x_c \approx 0.50$: the limit between the 3^+ and the 4^+ valence states for the U ions is not far away. Nevertheless, one has to note that both the 3^+ and the 4^+ ground states are magnetic, so a valence change alone does not explain the collapse of the magnetic ordering [7]. We note that the abnormal behaviour of U–La–S system cannot be only ascribed to a change in

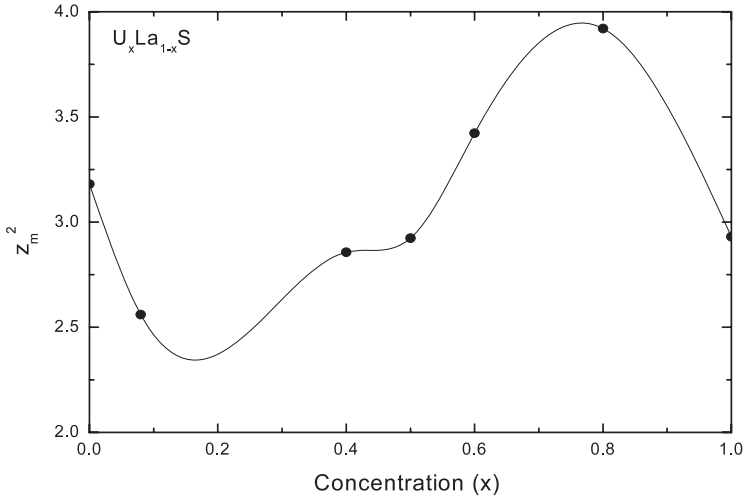

Figure 1. Variation of effective charge Z_{m}^2 with concentration (x) for $\mathrm{U}_x\mathrm{La}_{1-x}\mathrm{S}$.

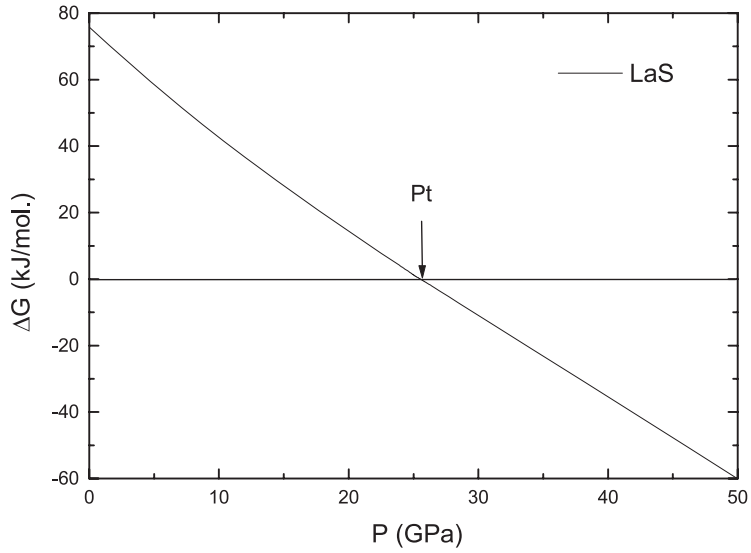

Figure 2. Variation of Gibbs free energy difference with pressure for LaS.

the 5f localization and actually the effects observed could also be related to a local distortion occurring in the S lattice. Another possibility is that there may be a metastable ordered phase around $x = 0.5$. The above argument needs a detailed study of the phase diagram and we shall address this in the near future. Two other short-range parameters, b and ρ, follow a linear trend of variation with x. However, Bihan *et al* [12] have earlier stressed that Vegard's law is not valid in the intermediate doping region.

In an attempt to reveal the structural phase transition of the $\mathrm{U}_x\mathrm{La}_{1-x}\mathrm{S}$ compounds, we minimize the Gibbs free energies $G_{\mathrm{B1}}(r)$ and $G_{\mathrm{B2}}(r')$ for the equilibrium interatomic spacing (r) and (r'). The Gibbs free energy difference $\Delta G[=G_{\mathrm{B2}}(r') - G_{\mathrm{B1}}(r)]$ has been plotted as a function of pressure (P) in figures 2–4 by using the interionic interaction potential

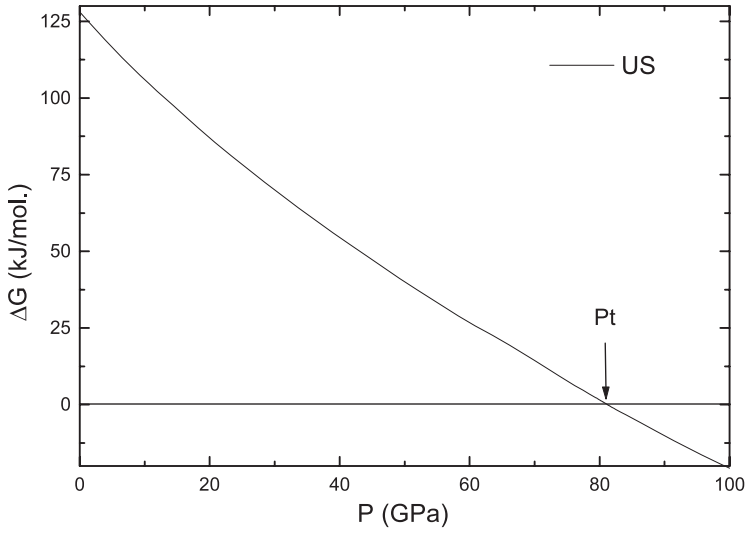

Figure 3. Variation of Gibbs free energy difference with pressure for US.

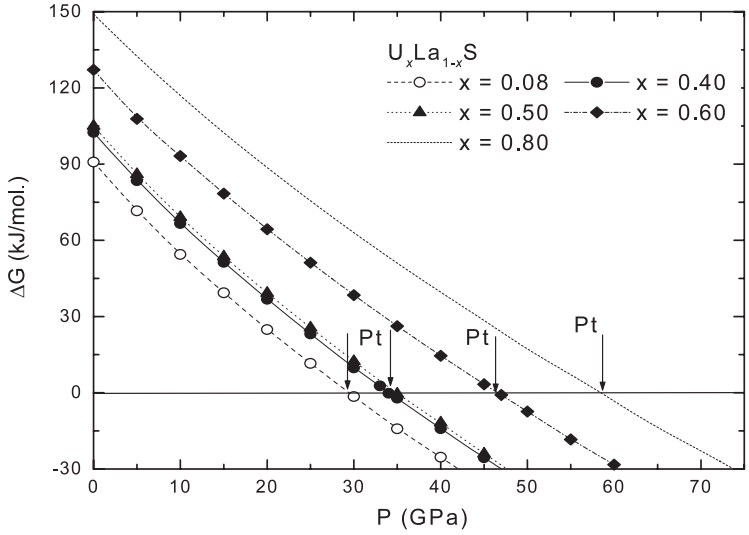

Figure 4. Variation of Gibbs free energy difference with pressure for $U_xLa_{1-x}S$.

discussed above. Let us summarize the results of the plots. The pressure corresponding to ΔG approaching zero is the phase transition pressure (P_t) (indicated by arrows in figures). At zero pressure, the B1 crystal is thermodynamically and mechanically stable, which is in agreement with the experimental result, and it will remain stable until the pressure reaches a value of about 25.5 (LaS), 30 ($U_{0.08}La_{0.92}S$), 34 ($U_{0.40}La_{0.60}S$), 35 ($U_{0.50}La_{0.50}S$), 47 ($U_{0.60}La_{0.40}S$), 59 ($U_{0.80}La_{0.20}S$) and 81 (US) GPa (transition pressure). At the transition pressure the thermodynamic potentials of both the phases are equal. As pressure increases, beyond the phase transition pressure (P_t), the thermodynamic potential of the B2 phase becomes lower, and hence this phase becomes mechanically and thermodynamically stable (its ΔG function value is more negative than that of B1 crystal).

Table 3. Calculated transition pressures and volume collapse of $U_xLa_{1-x}S$ compounds.

Compound		Transition pressure (GPa)	Volume collapse (%)
LaS	B1 → B2	25.5 (25[a], 24.9[b])	8.1 (8.4[b])
$U_{0.08}La_{0.92}S$	B1 → B2	30 (29[a])	7.6
$U_{0.40}La_{0.60}S$	B1 → B2	34 (32[a])	6.8
$U_{0.50}La_{0.50}S$	B1 → B2	35 (33[a])	6.8
$U_{0.60}La_{0.40}S$	B1 → B2	47 (45[a], 47[a])	7.1 (7.3[a])
$U_{0.80}La_{0.20}S$	B1 → B2	59 (56[a])	6.9
US	B1 → B2	81 (80[a])	4.7

[a] The quantities are experimental data, [12].
[b] The quantities are other theoretical work, [14].

For pressures higher than the theoretical thermodynamic transition pressure, the B1 crystal becomes thermodynamically unstable and the B2 phase remains stable up to the greatest pressure studied (≈100 GPa). In $U_xLa_{1-x}S$ compounds a crystallographic transition from B1 to B2 occurs. These results may be successfully compared with those available experimental data [12] and other theoretical work [14] and are listed in table 3. The estimated value of the P_t for LaS is in agreement with that obtained from the tight-binding linear muffin-tin orbital approach (TB-LMTO) [14]. In this sprit we point out that for $x \geqslant 0.60$, the high-pressure phase has yet to be determined and present EIoIP has correctly predicted the stable crystallographic structure as CsCl and a phase transition from B1 to B2 phase of $x = 0.80$ and 1.0. It is interesting to note that the transition pressure increases from LaS to US. The driving force of the structural phase transition is in this picture, seen as the hybridization of f orbitals with s- and p-like state. Furthermore, in the high-pressure phase of these compounds the f-electron localization increases from LaS to US, which may be the reason for the higher transition pressure. We should emphasize that our conclusions in $U_xLa_{1-x}S$ have been established only within the developed effective interionic interaction potential (lattice model) that we dealt with.

The pressure–volume relation of $U_xLa_{1-x}S$ was determined from Murnaghan equation of state that accounts for the values of the relative volumes $V(P)/V(0)$ associated with various compressions as [19]

$$\frac{V}{V_0} = \left(1 + \frac{B'}{B_0}P\right)^{-\frac{1}{B'}}, \tag{18}$$

where V_0 is the cell volume at ambient conditions, B_0 is the bulk modulus and B' its pressure derivative. The estimated value of the pressure-dependent radius for both the structures, the curve of volume collapse with pressure to depict the phase diagram is illustrated in figure 5. It is noticed from the plot that the present approach has predicted correctly the relative stability of competitive crystal structures, as the values of ΔG are positive. This is in agreement with the fact that a volume collapse occurs at the B1–B2 transition, and the U–U distances become smaller than the Hill limit [26], so the 5f bands can directly overlap and the f electrons are delocalized in $U_xLa_{1-x}S$. The magnitude of the discontinuity in volume at the transition pressure is obtained from the phase diagram and their values, tabulated in table 3, are in fairly good agreement with those revealed from experiments [12] and the tight-binding linear muffin-tin orbital approach (TB-LMTO) [14].

In order to complete the study of the high-pressure elastic behaviour of $U_xLa_{1-x}S$ compounds, we have computed the second-order elastic constants (SOECs) and their variation with pressure as shown in figure 6. We note that C_{44} decreases linearly with the increase of pressure away from zero at the phase transition pressures. In contrast, the values of C_{11} and C_{12} increase linearly with pressure. The above feature is quite similar to the earlier reported

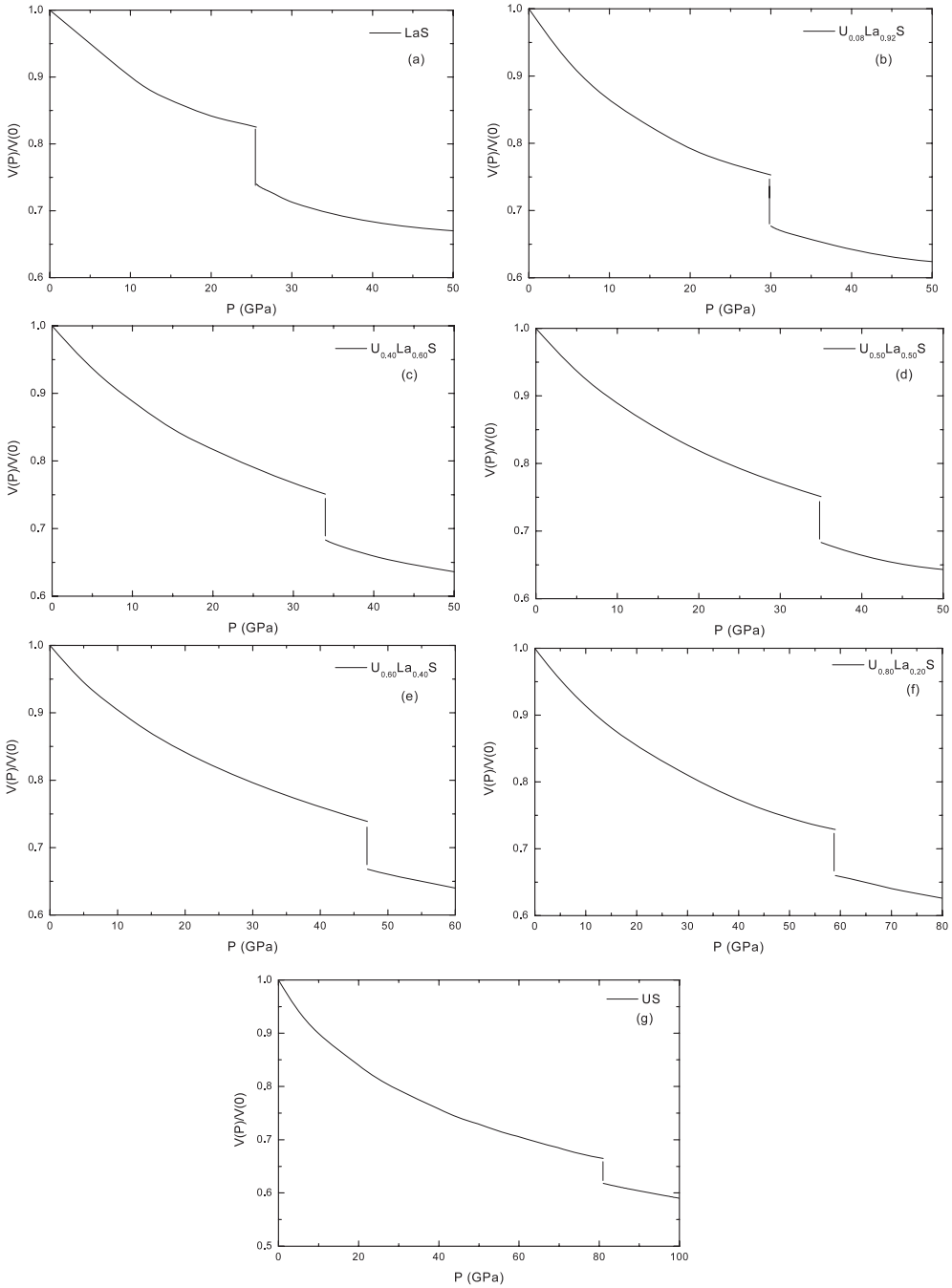

Figure 5. Pressure–volume diagram of $U_xLa_{1-x}S$.

pressure dependence of elastic stiffness for PbTe and SnTe possessing the NaCl structure with B1 to B2 structural phase transition [27]. Furthermore, the observed decrease in C_{44} suggested that softening of the lattice occurred with increasing in pressure. Softening of the same mode has previously been observed in the NaCl-type structure of MnO system [28]. It is instructive

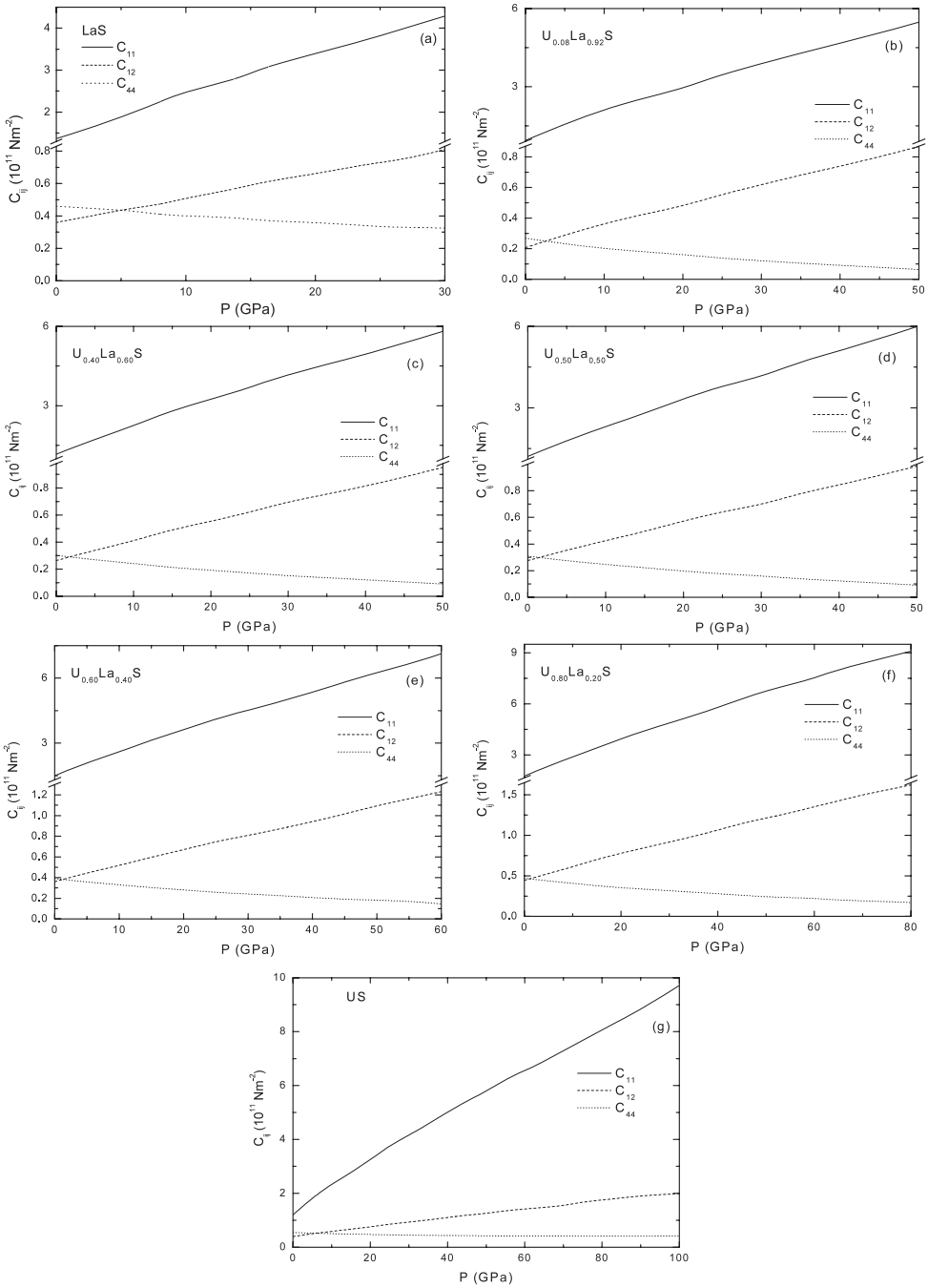

Figure 6. Variation of second-order elastic constants of $U_xLa_{1-x}S$ with pressure.

to mention that pressure-induced phonon softening has been found for the transverse acoustic (TA) branch as expected for the NaCl structure [29]. For better understanding, we plot the variation of the combination of SOECs elastic stiffness [$C_L = (C_{11} + C_{12} + 2C_{44})/2$] and shear moduli [$C_S = (C_{11} - C_{12})/2$] in figure 7. We observed that $C_L(C_S)$ increases linearly

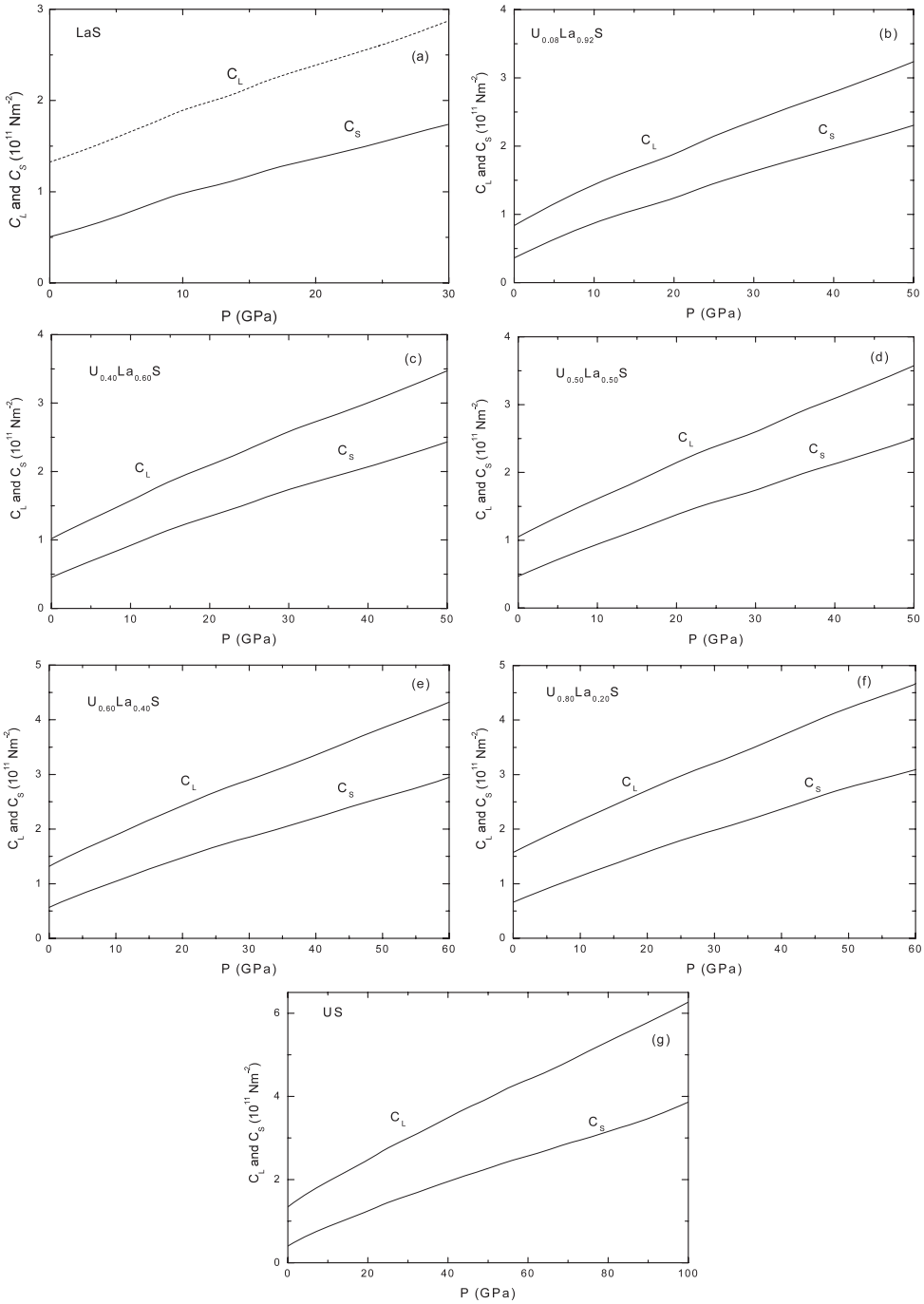

Figure 7. Variation of the combination of second-order elastic constants of $U_xLa_{1-x}S$ with pressure.

with increase in the pressure and in accordance with the first-order character of the transition for these compounds.

Table 4. Bulk modulus (B_T), shear modulus (C_{44}) and tetragonal modulus (σ) for $U_xLa_{1-x}S$ compounds.

Compounds	B_T (GPa)	C_{44} (GPa)	σ (GPa)
LaS	69 (89 ± 3)[a](107)[b]	46	50.5
$U_{0.08}La_{0.92}S$	45 (85 ± 2)[a]	26.9	36.6
$U_{0.40}La_{0.60}S$	56.5 (76 ± 4)[a]	30.2	45.1
$U_{0.50}La_{0.50}S$	58.7 (90 ± 1)[a]	30.8	46.8
$U_{0.60}La_{0.40}S$	73.9 (100 ± 2)[a]	39	56.8
$U_{0.80}La_{0.20}S$	88.3 (99 ± 3)[a]	47	65.9
US	66.1 (100 ± 1)[a]	54.6 (21 ± 1)[a]	40.2

[a] The quantities are experimental data, [12, 25].
[b] The quantities are from other theoretical work, [14].

In passing, we refer to the Born criterion of a lattice to be mechanically stable, which states that the elastic energy density must be a positive definite quadratic function of strain. The result is that the principal minors (alternatively the eigenvalues) of the elastic constant matrix should all be positive. The stability of a cubic crystal is expressed in terms of elastic constants as follows [13]:

$$B_T = (C_{11} + 2C_{12})/3 > 0, \tag{19}$$

$$C_{44} > 0, \tag{20}$$

and

$$\sigma = (C_{11} - C_{12})/2 > 0. \tag{21}$$

C_{ij} are the conventional elastic constants and B_T is the bulk modulus. The quantities C_{44} and σ are the shear and tetragonal moduli of a cubic crystal. Estimated values of bulk modulus, shear moduli and tetragonal moduli are tabulated in table 4, well satisfying the above elastic stability criteria for $U_xLa_{1-x}S$ compounds.

We refer to Vukcevich, who proposed a high-pressure stability criterion for ionic crystals, combining mechanical stability with minimum energy conditions [30]. In accordance, the stable phase of the crystal is one in which the shear elastic constant C_{44} is nonzero (for mechanical stability) and which has the lowest potential energy among the mechanically stable lattices. It is true that the agreement between the theoretical and the experimental value of B_T is not of the desired degree, but this may be because we have derived our expressions neglecting thermal effects and assuming the overlap repulsion significant only up to nearest neighbours in $U_xLa_{1-x}S$.

We now switch to discuss the elastic properties of doped uranium chalcogenides within the framework of developed interionic interaction potential. We have noticed that the shear elastic constant C_{44} is a very small quantity; the calculated value of $[(4r_0/e^2)C_{44} - 0.556Z_m^2]$ is found to be a negative quantity, so $(A_2 - B_2)$ is negative. This suggests that these terms belong to an attractive interaction and possibly arise due to the van der Waals energy. Based on this observation we suggest that the van der Waals energy converges quickly, but the overlap repulsion converges much more quickly.

The above fact implies that the second-neighbour forces in $U_xLa_{1-x}S$ are entirely due to the van der Waals interaction and the first-neighbour forces are the results of the overlap repulsion and the van der Waals attraction between the nearest neighbours. On the other hand, at high pressure the short-range forces for these compounds increase significantly, which, in turn, is responsible for the change in the coordination number and phase transformation. Other than deriving the equation of states correctly from a model approach and then analysing the

Table 5. The values of pressure derivatives of SOECs (dB_T/dP, dC_{44}/dP and dC_S/dP) and TOECs (C_{111}, C_{112}, C_{123}, C_{144}, C_{166} and C_{456}) (in units of 10^{11} N m^{-2}).

Quantities	LaS	$U_{0.08}La_{0.92}S$	$U_{0.4}La_{0.6}S$	$U_{0.5}La_{0.5}S$	$U_{0.6}La_{0.4}S$	$U_{0.8}La_{0.2}S$	US
dB_T/dP	4.52	8.59	8.50	8.48	8.49	8.47	4.06
dC_{44}/dP	−0.60	−0.12	−0.05	−0.04	−0.05	−0.11	−0.5
dC_S/dP	10.10	9.93	9.68	9.68	9.49	9.37	6.57
C_{111}	−30.5	−20.07	−24.54	−25.24	−30.74	−35.85	−23.24
C_{112}	−0.88	−0.48	−0.62	−0.64	−1.08	−1.074	−2.40
C_{123}	0.04	0.03	0.04	0.038	0.045	0.05	0.71
C_{144}	0.04	0.03	0.04	0.038	0.045	0.05	0.71
C_{166}	−0.79	−0.42	−0.54	−0.56	−0.87	−0.96	−2.50
C_{456}	0.09	0.06	0.08	0.08	0.095	0.12	0.66

variation of short-range forces, at present we have no direct means to understand the interatomic forces at high pressure.

We also analyse the anharmonic properties of $U_xLa_{1-x}S$ compounds by computing the third-order elastic constants (TOECs) and the pressure derivatives of SOECs at zero pressure [15]. The values of the pressure derivatives of SOECs (dC_S/dP, dB_T/dP and dC_{44}/dP) are listed in table 5. A reasonably good agreement with available experimental results for dB_T/dP has been obtained in all the cases under consideration. Also, the variation of TOECs with pressure is shown in figure 8. It can be seen that the variation of third-order elastic constants with pressure points to the fact that the values of C_{111}, C_{112}, C_{123}, C_{166}, C_{456} are negative while those of C_{144} are positive as obtained from the effective interionic potential at zero pressure. Thus, we can say that, in $U_xLa_{1-x}S$, the developed EIoIP consistently explains the high-pressure and elastic behaviour.

Apart from the phase transition and pressure dependence of SOECs in $U_xLa_{1-x}S$, we have also estimated the Debye temperature (θ_D) in the present approach. We define [13]

$$\theta_D^3 = \frac{3.15}{8\pi}\left(\frac{h}{k_B}\right)^3\left(\frac{r}{M}\right)^{\frac{3}{2}}[(C_{11}-C_{12})/2]^{1/2}[(C_{11}+C_{12}+2C_{44})/2]^{1/2}[C_{44}]^{1/2}. \tag{22}$$

Here, M is the acoustic mass of the compounds, and h and k_B are the Planck and Boltzmann constants, respectively. It is inferred for figure 9 that θ_D varies linearly with pressure for all the compounds and this is attributed to softening of the lattice with pressure. The calculated values of the Debye temperature at zero pressure are consistent with the reported data, 255 K (235.4 [14], 276 [31] K) for LaS and 235 K (239 [32], 205 ± 2.5 [33] K) for US, respectively.

We do not claim the process to be rigorous, but an agreement following the EIoIP consistent with experiments and other work is obtained on the Debye temperature. A systematic decrease in θ_D is noticed with increasing U doping concentration; however, due to large value of B_T, US does not follow the systematic trend, being the end member of the series. The reason for above needs careful study of heat capacity behaviour in these compounds to address why US and LaS are so different from other intermediate phases. Usually, the Debye temperature is also a function of temperature, and it varies from technique to technique and depends on the sample quality with a standard deviation of about 15 K.

One approximates that this result motivates the definition of an 'average' elastic constant as

$$C = \left(\frac{8\pi}{3.15}\right)^{\frac{2}{3}}\left(\frac{k_B}{h}\right)^2\left(\frac{M}{r}\right)\theta_D^2, \tag{23}$$

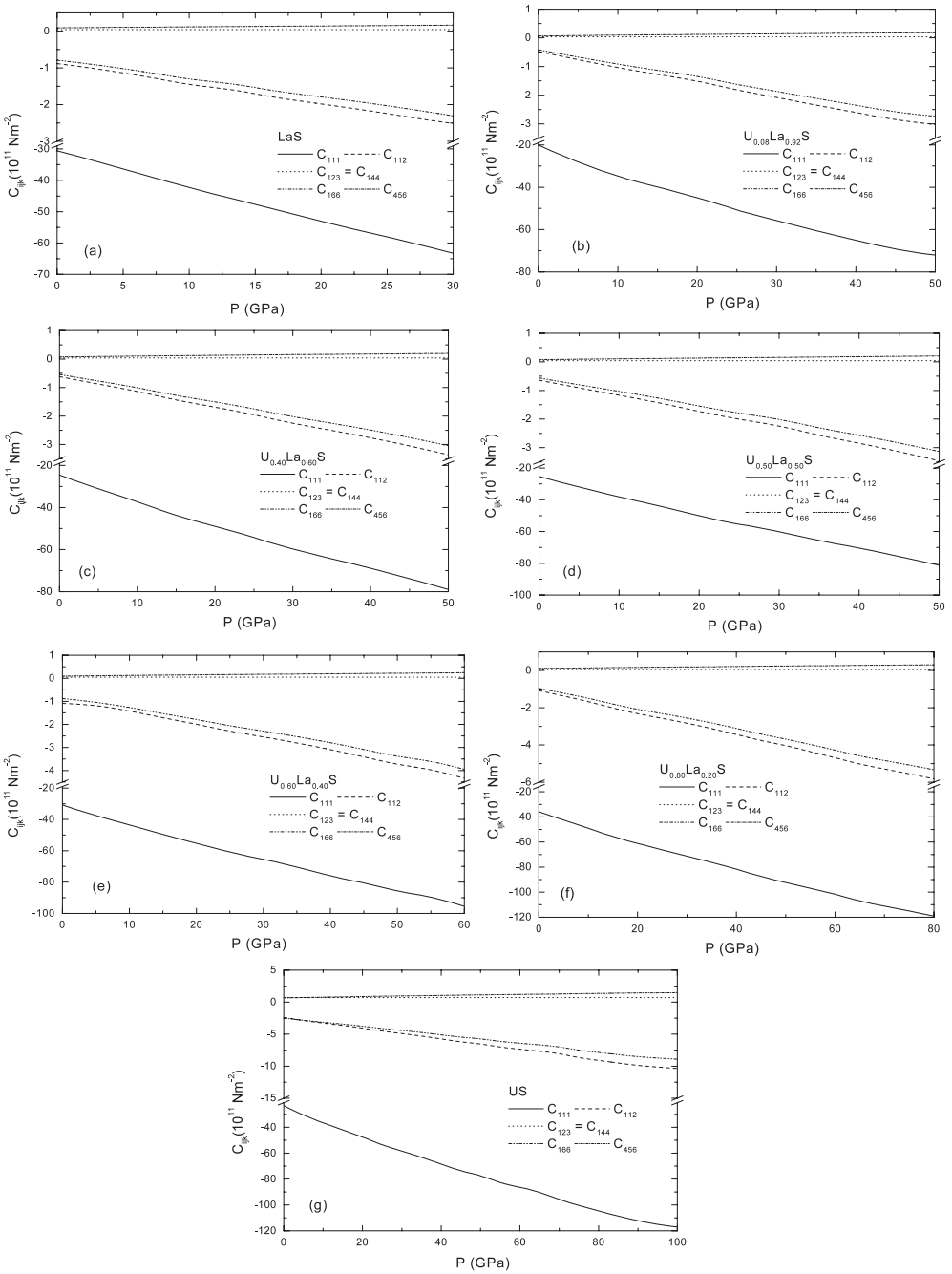

Figure 8. Variation of third-order elastic constants of $U_xLa_{1-x}S$ with pressure.

which in turn is calculated from the Debye temperature and allows us to correlate the Cauchy discrepancy in the elastic constant as follows

$$C^* = \frac{C_{12} - C_{44}}{C_{12} + C_{44}}, \tag{24}$$

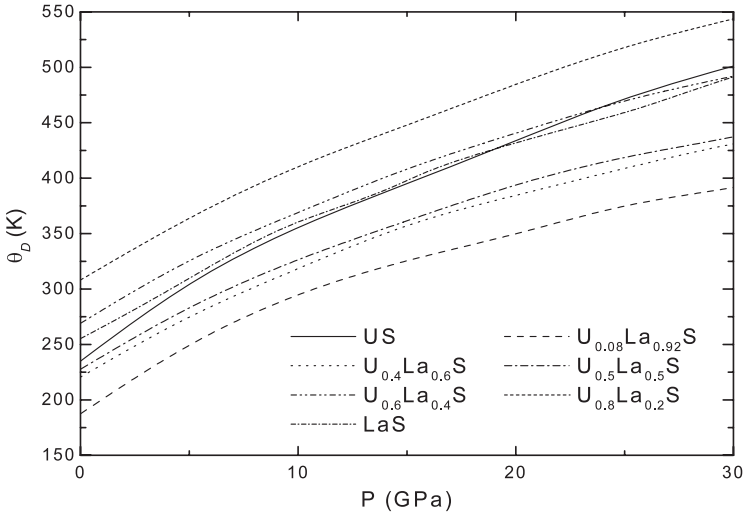

Figure 9. Variation of Debye temperature θ_D of $U_xLa_{1-x}S$ with pressure.

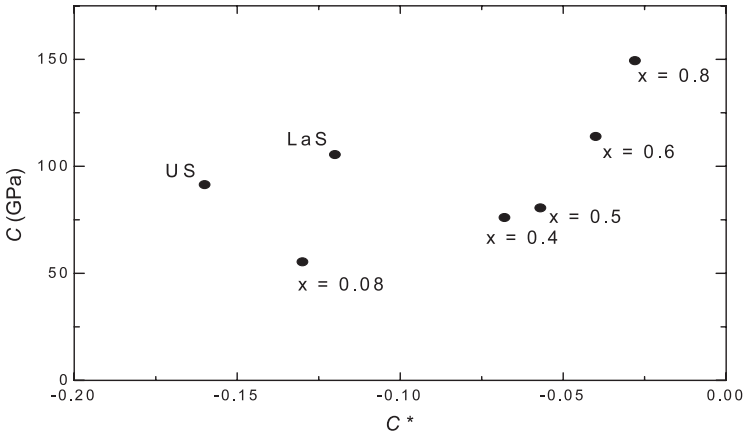

Figure 10. The 'average' elastic constant C as a function of Cauchy discrepancy of $U_xLa_{1-x}S$ compounds.

at zero pressure. Figure 10 shows the variation of 'average' elastic constant (C) with Cauchy discrepancy (C^*) for $U_xLa_{1-x}S$ compounds. It is worth mentioning that C_{44} is larger as compared to C_{12}, which is consistent with the available experimental data on PbTe and SnTe possessing the NaCl structure with B1 to B2 structural phase transition [27]. However, we note that the rare-earth monochalcogenides with NaCl-type structure (B1 to B2 structural phase transition) [13] and diluted magnetic semiconductors with zinc blende structure (B3 to B1 structural phase transition) [34] and most of the body-centred cubic transition metals shows a positive Cauchy deviation C^*.

4. Conclusions

To determine the stable structure at finite pressure and temperature, the Gibbs free energy should be considered; the structure with lowest free energy is the most stable. The

realistic description of structural and mechanical properties needs to take into account various interactive forces when the lattice is strained and a balance of them to attend the stable structure depending upon the ionic nature. With this idea we have therefore calculated the pressure-induced structural and elastic properties of $U_xLa_{1-x}S$ solid solutions with stable rock salt structures by considering various interionic interactions. As an approximation and simplification, the temperature has been set to zero so that the entropy of the crystal is therefore ignored. This is in the spirit of the fact that the contribution of temperature to the free energy is small for the experimental data considered.

An effective interionic interaction potential is formulated in analysing the structural as well as elastic properties in $U_xLa_{1-x}S$ compounds. The trivalent phase of the U monochalcogenides becomes relevant at high pressure and the substituted compounds show a first-order phase transition towards a CsCl-type phase at a critical pressure. It is worth mentioning that the CsCl structure favours the f–f mixing processes, and hence the formation of f bands, because the U–U distance in the CsCl structure is shorter than in the NaCl structure, whereas the opposite holds for the U–anion distance. Thus, it is likely that the delocalization of f electrons is produced mainly by hybridization with anion orbitals at the ambient pressure phase, and mainly by the formation of f bands in the high-pressure phase.

The obtained values of material parameters allow us to predict the phase transition pressure and associated volume collapse. The results of the lattice model calculations yield the phase transition pressure of 25.5 (LaS), 30 ($U_{0.08}La_{0.92}S$), 34 ($U_{0.40}La_{0.60}S$), 35 ($U_{0.50}La_{0.50}S$), 47 ($U_{0.60}La_{0.40}S$), 59 ($U_{0.80}La_{0.20}S$) and 81 (US) GPa. For all these compounds excellent agreement is found with available data on the phase transition pressure. Also all these compounds from the vast volume discontinuity in pressure–volume phase diagram identify the B1 $\rightarrow$ B2 structural phase transition. The good agreement both for transition pressures and volume collapses shows that in the rock salt phase the localized f^3 U ions coexist with a partly occupied narrow f band, effectively describing an intermediate valence phase. The model's ability to predict realistic cohesive properties such as the equilibrium volume, the bulk modulus, its derivative with pressure, the relative stability of crystal structures, and transition pressures and volumes is exemplified in terms of the screening of the effective Coulomb potential through the modified ionic charge (Z_m^2). Usually the delocalization of f electrons indeed will result in a change in Coulomb screening, but, in contrast, one cannot attribute a variation of effective charge solely to f electrons.

The lattice model calculations also support the validity of the Born criterion. The second-order elastic constants C_{11} and C_{12} increase with increase in pressure up to the phase transition pressure that identifies the high-pressure structural stability of $U_xLa_{1-x}S$ compounds. Further, C_{44} decreases linearly with the increase of pressure and does not tend to zero at the phase transition pressures and is in accordance with the first-order character of the transition.

Conclusively, the proper incorporation of the realistic physical parameters based on the experimental observations will allow us to interpret a consistent pressure-induced structural transformation of rare-earth-doped uranium monochalcogenides. However, the deviations might be ascribed to the extension of the covalent and zero-point motion effects. Nevertheless, it has been found that this simple model as compared to complicated band structure calculations may account for a considerable part of the available experimental and theoretical results of the high-pressure studies.

Acknowledgment

Financial support from UGC, New Delhi is gratefully acknowledged.

References

[1] Vogt O, Mattenberger K and Löhle J 2001 *J. Magn. Magn. Mater.* **231** 199
[2] Reihl B, Martensson N and Vogt O 1982 *J. Appl. Phys.* **53** 2008
[3] Schoenes J 1998 *J. Alloys Compounds* **275–277** 148
[4] Johansson B and Brooks M S S 1993 *Handbook on the Physics and Chemistry of Rare Earths* vol 17, ed K A Gschneidner Jr, L Eyring, G H Lander and G R Choppin (Amsterdam: Elsevier) p 1
Brooks M S S, Johansson B and Skriver H L 1984 *Handbook on the Physics and Chemistry of the Actinides* vol 1, ed A J Freeman and G H Lander (Amsterdam: North-Holland) p 153
[5] Sheng Q G and Cooper B R 1996 *J. Magn. Magn. Mater.* **164** 335
[6] Grosse G, Kalvius G M, Kratzer A, Schreier E, Burghart F J, Mattenberger K and Vogt O 1999 *J. Magn. Magn. Mater.* **205** 79
[7] Schoenes J, Vogt O, Löhle J, Hulliger F and Mattenberger K 1996 *Phys. Rev.* B **53** 14987
[8] Sheng Q G, Cooper B R and Lim S P 1994 *Phys. Rev.* B **50** 9215
[9] Sheng Q G and Cooper B R 1995 *Phil. Mag. Lett.* **72** 123
[10] Cooper B R, Vogt O, Sheng Q G and Lin Y-L 1999 *Phil. Mag. Lett.* **79** 683
[11] Cooper B R, Lin Y-L and Sheng Q G 1999 *J. Appl. Phys.* **85** 5338
[12] Le Bihan T, Bombardi A, Idiri M, Heathman S and Lindbaum A 2002 *J. Phys.: Condens. Matter* **14** 10595
[13] Varshney D, Kaurav N, Kinge R and Singh R K 2007 *J. Phys.: Condens. Matter* **19** 236204
Varshney D, Kaurav N, Kinge R, Shah S and Singh R K 2005 *High Pressure Res.* **77** 1075
Varshney D, Kaurav N, Sharma P, Shah S and Singh R K 2004 *Phys. Status Solidi* b **241** 3179
[14] Vaitheeswaran G, Kanchana V and Rajagopalan M 2003 *J. Phys. Chem. Solids* **64** 15
[15] Singh R K 1982 *Phys. Rep.* **85** 259
[16] Hafemeister D W and Flygare W H 1965 *J. Chem. Phys.* **43** 795
[17] Tosi M P 1964 *Solid State Phys.* **16** 1
[18] Huggins M L and Sakamoto Y 1957 *J. Phys. Soc. Japan* **12** 241
[19] Varshney D, Kaurav N, Sharma P, Shah S and Singh R K 2004 *Phase Transit.* **77** 1075
Varshney D, Kaurav N, Sharma U and Singh R K 2006 *J. Alloys Compounds* at press
Varshney D, Sharma P, Kaurav N and Singh R K 2005 *Bull. Mater. Sci.* **28** 651
Varshney D, Kinge R, Sharma P, Kaurav N and Singh R K 2005 *Ind. J. Pure Appl. Phys.* **43** 939
Varshney D, Sharma P, Kaurav N, Shah S and Singh R K 2004 *Phys. Status Solidi* b **241** 3374
[20] Slater J C and Kirkwood J G 1931 *Phys. Rev.* **37** 682
[21] Euiot R J and Leath R A 1976 *Dynamical Properties of Solids* vol II, ed G K Horton and A A Maraduddin (New York: Academic) p 386
[22] Vegard L 1921 *Z. Phys.* B **5** 17
[23] Lide D R (ed) 1999 *CRC Handbook of Chemistry and Physics* 79th edn (New York: CRC Press)
[24] Nakayama M, Ito T, Kumigashira H, Matsui H, Komatsu H, Takahashi T, Aoki H and Ochiai A 2004 *J. Magn. Magn. Mater.* **272–276** E121
[25] Jackman J A, Holden T M, Buyers W J L, DuPlessis P de V, Vogt O and Genossar J 1985 *Phys. Rev.* B **33** 7144
[26] Hill H H 1970 *Plutonium 1970 and other Actinides* (*AIME Nuclear Metallurgy Series*) vol 17, ed W H Miner (New York: Metallurgical Society AIME) p 2
[27] Miller A J, Saunders G A and Yogurtcu Y K 1981 *J. Phys. C: Solid State Phys.* **14** 1569
[28] Webb S L, Jackson I and Fitz Gerald J D 1988 *Phys. Earth Planet. Inter.* **52** 117
[29] Anderson O L and Liebermann R C 1981 *Phys. Earth Planet. Inter.* **3** 61
[30] Vukcevich M R 1972 *Phys. Status Solidi* b **54** 435
[31] Bucher E, Andres K, Disalvo F J, Maita J P, Gossard A C, Cooper A S and Hull G W 1975 *Phys. Rev.* B **11** 500
[32] Westrum E F, Walters R R Jr, Flotow H E and Osborne D W 1968 *J. Chem. Phys.* **48** 155
[33] Rudigier H, Ott H R and Vogt O 1985 *Phys. Rev.* B **32** 4585
[34] Varshney D, Sharma P, Kaurav N, Shah S and Singh R K 2005 *J. Phys. Soc. Japan* **74** 382